Metasurface Device with Helicity-Dependent Functionality

Metasurface Device with Helicity-Dependent Functionality

Dandan Wen, Shumei Chen, Fuyong Yue, Kinlong Chan, Ming Chen, Marcus Ardron, King Fai Li, Polis Wing Han Wong, Kok Wai Cheah, Edwin Yue Bun Pun, Guixin Li, Shuang Zhang,* and Xianzhong Chen**

Driven by miniaturization and system integration, ultrathin, multifunction optical elements are urgently needed. Traditional polarization-selective optical elements are mainly based on birefringence, which is realized by using the well-designed structure of each phase pixel. However, further reduction of the pixel size and improvement of the phase levels are hindered by the complicated fabrication process. An approach is proposed to realize a metasurface device that possesses two distinct functionalities. The designed metasurface device, consisting of gold nanorods with spatially varying orientation, has been experimentally demonstrated to function as either a lens or a hologram, depending on the helicity of the incident light. As the phase of the scattered light is controlled by the orientation of the nanorods, arbitrary phase levels and dispersionless phase profile can be realized through a much simpler fabrication process than the conventional device. This approach provides an unconventional alternative to realize multifunction optical element, dramatically increasing the functionality density of the optical systems.

1. Introduction

Miniaturization and integration are two continuing trends in the production of photonic devices. Great effort has been made to incorporate multifunctions into a single device,[1–3] such as the optical Janus device.[4] As one of the important multifunction optical elements, polarization selective optical elements (PSOE) can achieve multiple functionalities according to the polarization states of the incident beam; these have been applied in optical encryption,[5] image processing,[6] and so on. To construct PSOEs, two anisotropic substrates[7,8] or a structure with form-birefringent[9,10] have been traditionally used to impose the desired phase delay for the two cross-polarizations of incident light. Although these devices prove to be effective, it is challenging for the etching depth control especially when some extreme phase profiles are needed. Besides, these devices suffer from the limited phase levels and the large pixel size due to the current fabrication techniques.

Benefiting from the easy fabrication and the flexible control of the light propagation, metasurfaces have provided new opportunities to realize virtually flat optics.[11–26] In comparison with the traditional PSOEs, which realize the birefringence by carefully designing the structure of each pixel, the metasurface provides a much easier way by directly merging different optical elements together with each one working for a particular incident polarization. Reflective-type metasurface holograms have been demonstrated to reconstruct two interchangeable images[27,28] by controlling the linear polarization state of the incident light. Although the previously proposed metasurfaces have shown their unique advantages such as broadband[27] and wide field of view,[28] further application is hindered by the limited phase levels[27] and binary modulation[28] of the holograms since most optical elements such as a lens or an axicon are required to precisely manipulate the phase of the wavefront.

D. Wen, F. Yue, Prof. M. Chen, Prof. X. Chen
SUPA, Institute of Photonics and Quantum Sciences
School of Engineering and Physical Sciences
Heriot-Watt University
Edinburgh EH14 4AS, UK
E-mail: x.chen@hw.ac.uk

Dr. S. Chen, K. Chan, Dr. K. F. Li, Prof. K. W. Cheah, Dr. G. Li
Department of Physics
Hong Kong Baptist University
Kowloon Tong, Hong Kong
E-mail: guixinli81@gmail.com

Prof. M. Chen
Guangxi Experiment Center of Information Science
Guilin University of Electronic Technology
Guilin 541004, China

Dr. M. Ardron
Renishaw PLC
Research Avenue North
Riccarton, Edinburgh EH14 4AP, UK

Dr. P. W. H. Wong, Prof. E. Y. B. Pun
Department of Electronic Engineering
City University of Hong Kong
83 Tat Chee Avenue, Hong Kong

Prof. E. Y. B. Pun
State Key Laboratory of Millimeter Waves
City University of Hong Kong
83 Tat Chee Avenue, Hong Kong

Dr. G. Li, Prof. S. Zhang
School of Physics and Astronomy
University of Birmingham
Birmingham B15 2TT, UK
E-mail: s.zhang@bham.ac.uk

DOI: 10.1002/adom.201500498

In this paper, we propose and experimentally verify a novel method to realize a metasurface device that possesses two distinct functionalities. The realization of each functionality depends on the helicity of the incident light. As shown in **Figure 1**, the metasurface device acts as a hologram when the polarization state of the incident light is left circular polarization (LCP), while the same device will turn into a convex lens when the polarization state is changed to right circular polarization (RCP). Arbitrary phase levels of the phase-only metasurface can be realized with an easy-to-fabricate process, which is highly desirable for the phase modulation optical elements. Since the helicity of the incident light can be controlled, the additional degrees of freedom provided by Berry phase can be used to integrate two independent optical elements into a single metasurface. To maintain the unique characteristics of conventional optical elements which usually alter the phase front only in the propagation direction, we demonstrate the capability of the multifunction metasurface device along this direction. In addition, the proposed metasurface device is ultrathin (≈40 nm) and broadband, which can dramatically increase the functionality density in the integrated optical systems. In this work, we integrate two optical devices with totally different functionalities on the single transmission-type device with functionality-switchable property. As a brand new optical device, our work might not only trigger the interest of the general public in the science and technology enabled by metamaterials and metasurfaces but also can contribute to future possibilities for applications in the relevant research fields.

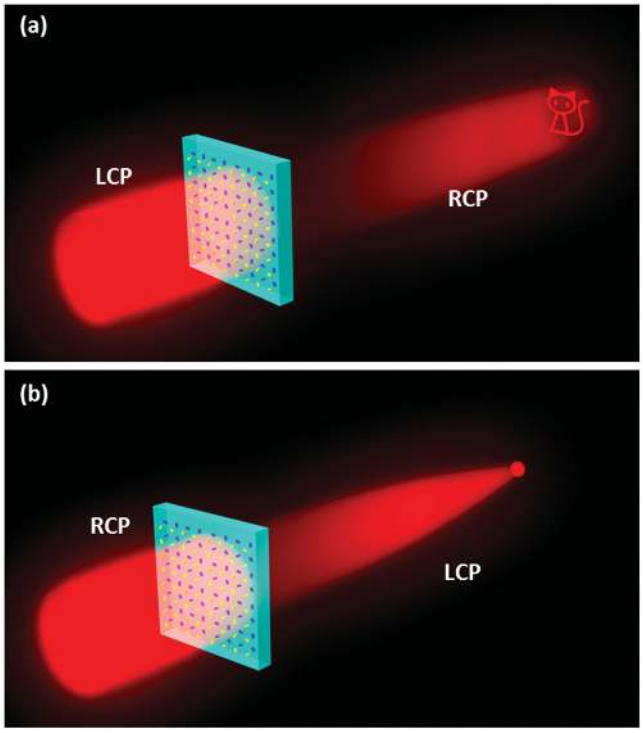

Figure 1. Schematic to show the polarization selectivity of the metasurface device. The metasurface functions as a) a hologram to reconstruct an image of "cat" or b) a lens that converges the incident light into the focal point, depending on the incident/detected light combination.

2. Materials and Methods

To create the helicity dependent multifunction metasurface device, a 2D array of gold nanorods fabricated on the ITO (indium tin oxide) coated glass substrate is utilized. Each nanorod functions like an anisotropic scatterer,[29] i.e., the complex scattering coefficients for the incident light polarized along the two axes of the nanorod are different. As a result, the nanorod is capable of converting the circularly polarized (CP) incident light into two parts: one has the same polarization as that of the incident light and no phase shift and the other one has the opposite polarization of the incident light and an abrupt phase change of $\pm 2\phi$, where ϕ is the orientation of the nanorod. The "+" or "−" depends on the combination the input/detected polarization, with the "+" sign for LCP/RCP and the "−" sign for RCP/LCP.[30–34] The conversion efficiency of a nanorod for changing the incident light into the opposite helicity is determined by its geometry,[35] which implies that a phase function can be encoded onto the metasurface consisting of nanorods with spatially varying orientations.

First, a phase-only hologram for the target image of "cat" is generated. The target image is discretized and regarded as a collection of point sources. After each point source is added with a random phase, the phase-only hologram is obtained by superimposing the light emitting from all the point sources (see Section 1 in the Supporting Information). Then the phase distribution of the hologram is sampled and encoded onto the metasurface. Each nanorod defined in the metasurface represents a sampled phase value in the hologram. Under the illumination of LCP light, the desired continuous local phase profile is generated for the transmitted RCP light and the image "cat" is reconstructed (**Figure 2**a). Similarly, by encoding the phase function of $\phi(x,y) = -(2\pi/\lambda)\left(\sqrt{x^2+y^2+f^2} - f\right)$ onto the metasurface,[36] a convex lens with the focal length f is created for the incident/detected combination of RCP/LCP. However, the metasurface lens turns into concave when the combination changes to LCP/RCP[12] and the refracted light diverges as though it is emanated from a virtual image plane on the incident side of the metasurface (Figure 2b). Finally, the two sets of data are merged together with a displacement vector of $(d/2, d/2)$ (Figure 2c), where d is the distance between neighboring nanorods. Although the merged metasurface contains nanorods of two categories, the size of the sample is still the same and the equivalent pixel size changes into $\sqrt{2}d/2$ (viewing from the 45° direction), leading to the increase of the nanorod density.

The two types of nanorods contributing to the hologram and the lens are named type A and type B for convenience, respectively. As the dipolar coupling between the neighboring nanorods is negligible,[37] the nanorods of the two categories work independently. For the incident/detected combination of LCP/RCP, the RCP light emitting from the nanorods A reconstructs the image of "cat," and the RCP light from the nanorods B diverges and forms a subtle background Figure 2c). In contrast, if the combination is switched to RCP/LCP, the phase profiles of the metasurface in Figure 2a–c are all reversed and the merged metasurface changes from a hologram to a convex lens (Figure 2d–f). By comparing Figure 2c with Figure 2f, it clearly shows that the functionality of the merged metasurface is switchable, depending on the incident/detected combination.

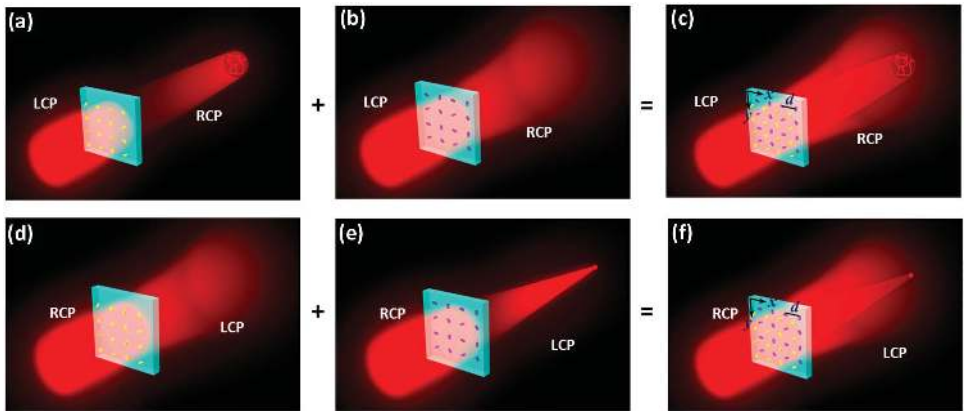

Figure 2. Design methodology for obtaining two distinct functionalities on a single metasurface device. Two different metasurfaces consisting of a) a hologram that can reconstruct a real image of "cat" and b) a concave lens that diverges the refracted beam for the incident/detected combination of LCP/RCP. c) The two metasurfaces are merged together with a displacement vector of (d/2, d/2). Only a reconstructed image of "cat" is observed upon the illumination of LCP. As the polarity of the hologram and the lens depend on the polarization of the incident light, no real image is observed in (d) but a real focal point appears in (e) when the incident/detected combination is changed from LCP/RCP to RCP/LCP. f) Similarly, a focal point will be observed in the real focal plane of the designed metasurface.

3. Results

First, we calculate the phase profiles for the hologram and the lens separately, then merge them together and encode onto the metasurface (**Figure 3**a). The metasurface is fabricated on the ITO coated glass substrate with the standard electron beam lithography, followed by the gold film deposition and lift-off process (see Section 2 in the Supporting Information). The scanning electron microscopy image of the fabricated metasurface is shown in Figure 3b. The incident CP light is generated by a polarizer and a quarter-wave plate, which are placed in front of the spectrally tunable laser source (NKT, SuperK Extreme). The fabricated sample is mounted on the 2D translational stage with the metasurface side facing the incident light. To ensure the uniform illumination of the metasurface, the incident beam has a diameter (≈2 mm) much larger than the size of the metasurface (400 μm). The scattered light in the transmission side is collected by an objective (10×/0.3) and a lens (f = 50 mm) that used for the far-field microscopy detection. As the objective is fixed on the 3D translational stage whose resolution along the optical path is 1 μm, the distance between the objective and the metasurface can be finely adjusted. Another pair of quarter-wave plate and polarizer is placed in the transmission side to select the CP light with opposite helicity to the incident light. Finally, the amplified images are captured by a CCD (charge-coupled device) camera.

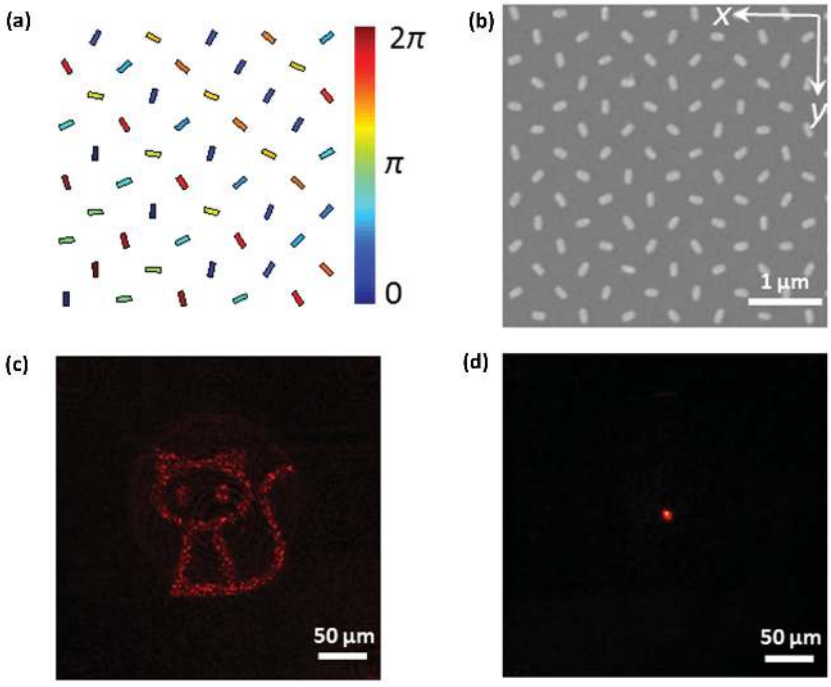

Figure 3. Metasurface encoding process and the experimental results. a) Nanorod distribution for part of the designed multifunction metasurface device. The phases of the nanorods are denoted by the different colors. The metasurface has the size of 400 μm × 400 μm in total and the sampling number is 666 × 666 × 2 (666 × 666 for the hologram and the same for the lens). The target image of "cat" is designed to be 150 μm × 150 μm in size and the reconstruction distance is 200 μm. The focal length of the lens is 200 μm. b) Part of the scanning electron microscope image of the fabricated metasurface. The gold nanorods are fabricated on the ITO coated glass substrate with a standard electron-beam lithography and lift-off process. Each nanorod is 50 nm wide, 150 nm long, and 40 nm high. The nanorods in odd and even rows contribute to the lens and hologram, respectively. The distance between the neighboring nanorods is 600 nm both in the x and y directions. c) When the incident/detected light is LCP/RCP, the merged metasurface functions as a hologram and the image of "cat" is reconstructed experimentally. d) When the incident/detected light (633 nm) is RCP/LCP, the metasurface turns into a lens that converges the refracted light to the focal point.

The polarization selectivity of the metasurface is experimentally verified. The metasurface functions as a hologram when the incident/detected polarization combination has the state of LCP/RCP (Figure 3c). By gradually tuning the distance between the objective and the metasurface, the optical intensity distribution is examined along the propagation direction to determine the position of the image "cat." When the polarizations of the incident and detected beams are switched to RCP and LCP, respectively, the metasurface functions as a convex lens that causes the incident laser beam to converge at a focal plane on the transmission side (Figure 3d). In comparison with Figure 3c, it clearly shows that the selectivity of the metasurface from the hologram to the convex lens is solely attributed to the helicity change of the CP light for the incident/detected combination, which is in good agreement with the theoretical prediction.

Since the phase profile of the metasurface is only determined by the orientation of the nanorods and the helicity of the incident light, the metasurface is expected to work over a wide range of wavelengths. The broadband property of the metasurface is verified by the images captured at different wavelengths from 533 to 733 nm with an interval of 50 nm (see Section 3 in the Supporting Information). As the designed metasurface possesses two functionalities, a detailed performance analysis of two separate functionalities is given in the following. Huygens' principle is used to simulate the reconstructed images since the full wave numerical simulation of the designed device is beyond our simulation capability due to the large array of antennas contained in the metasurface device. The simulated and experimentally obtained holographic images are shown in **Figure 4**a,b, respectively. In comparison with Figure 4a, the background noise (intensity in areas A and C) increases and the fineness of the image degrades in Figure 4b. The signal-to-noise ratio (SNR) defined as I_B/S_A is also analyzed. I_B is the mean intensity value within area B and S_A is the standard deviation of area A. The SNR is 10.51 in Figure 4a and 7.97 in Figure 4b. The mismatch between the experimental results and simulation is mainly due to the fabrication uncertainty (e.g., missing dipoles), where any deviation from the designed phase values can increase the background noise.[38] Nevertheless, the pattern outline is still sharp enough to generate a clear image. The beam propagation characteristics when the metasurface functions as a convex lens are analyzed in **Figure 5**. Figure 5a shows the experimentally obtained CCD images of the light spots corresponding to the positions A–E in the beam path, where the point C represents the focal point. Figure 5b is the corresponding normalized intensity distribution in Figure 5a. It can be seen that the beam size (characterized by the full width at half maximum) along the propagation direction is almost symmetric about the focal point, which agrees with the theoretical prediction. The beam size of the focal point is ≈6.5 μm representing an effective compression of the original incident beam. Due to the resolution of the measurement system (1.06 μm at λ = 633 nm), the measured beam size is larger than the calculated value.[39] Moreover, benefiting from the submillimeter size and the short focal length, the metasurface lens has a high numerical aperture of 0.707.

4. Discussion

One of important parameters that can be used to evaluate the performance of the designed metasurface is conversion efficiency, which is defined as the ratio of the power of the

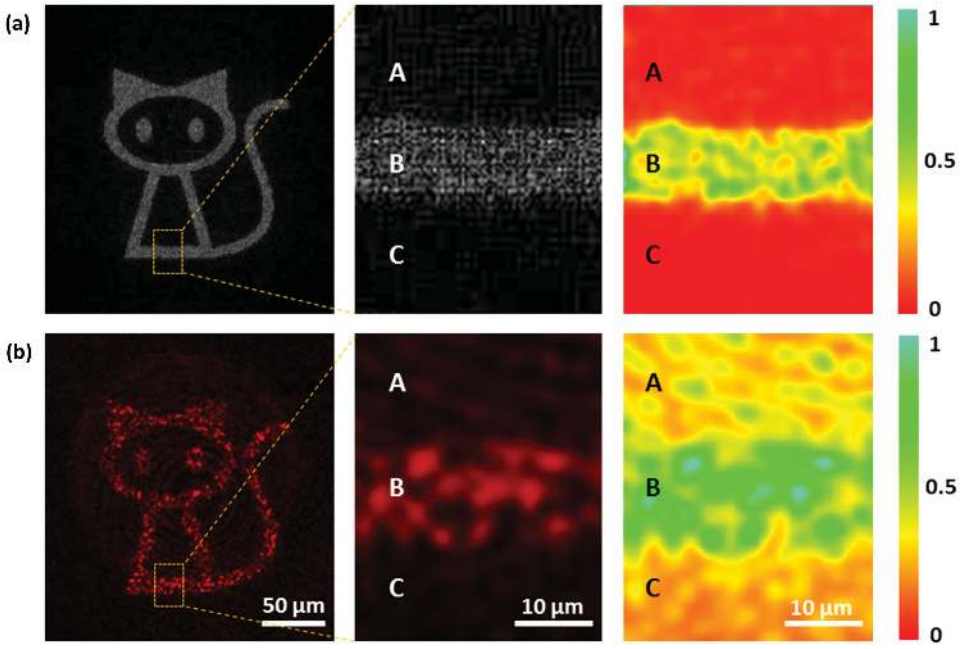

Figure 4. Detailed analysis of the reconstructed images when the merged metasurface functions as a hologram. The left row shows a) the simulated and b) experimentally reconstructed images of "cat" for the designed metasurface device at the wavelength of 633 nm. Areas A, B, and C are marked out in the reconstructed images. Area B is a portion of the reconstructed "cat," while areas A and C exclude the reconstructed image and are located beside area B. The zoom-in images and the normalized intensity distribution of the areas A–C are shown in the middle and right columns, respectively.

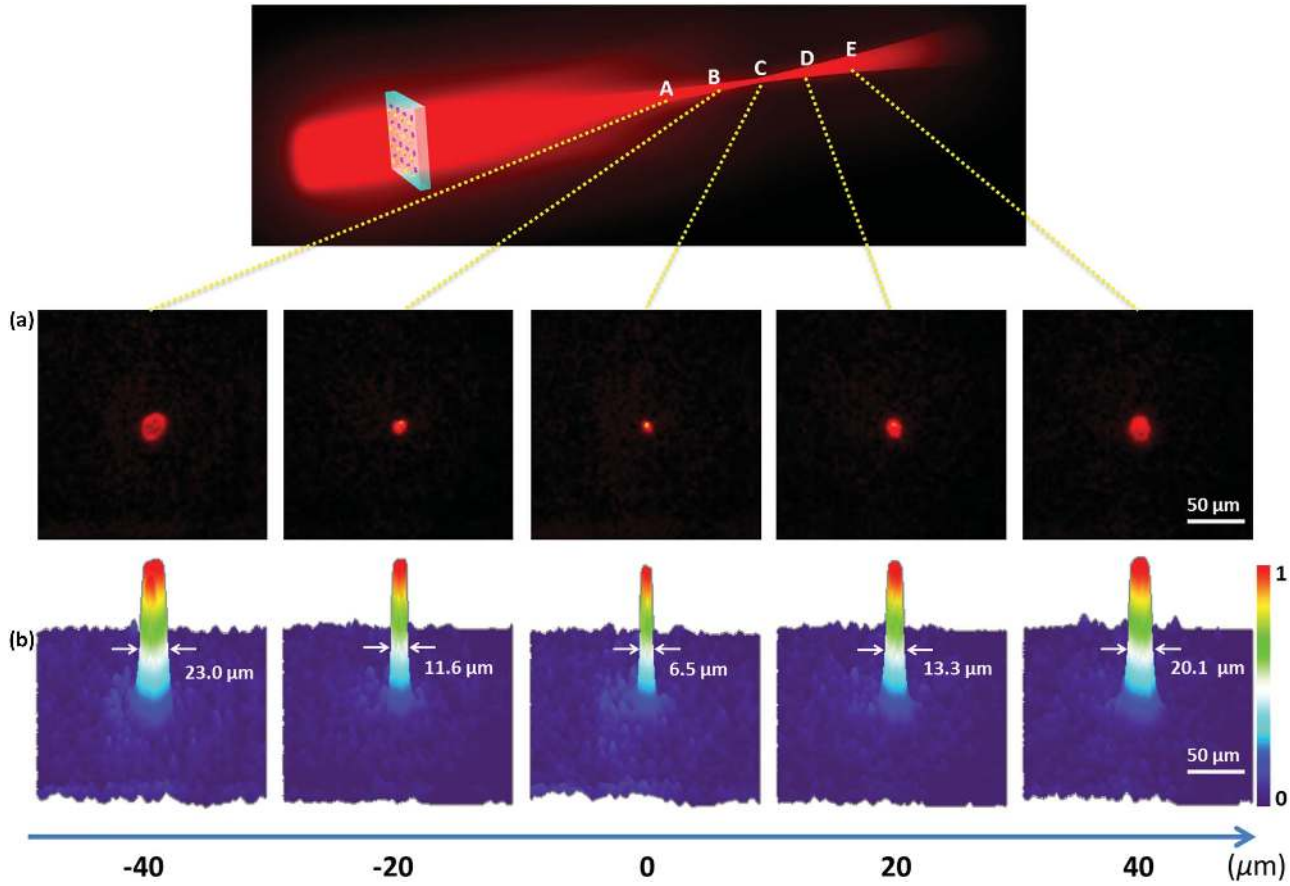

Figure 5. The light propagation characteristics when the metasurface functions as a convex lens. a) Experimentally obtained CCD images of the light spots at different planes A–E along the longitudinal direction. The distance between two neighboring planes is 20 μm and C is the focal plane. b) The corresponding normalized intensity distribution in (a). The full width at half maximum of each light spot is measured and labeled.

transmitted light with opposite helicity to that of the incident circularly polarized light. The maximum conversion efficiency we obtained in the experiment is 5% at the wavelength of 880 nm (details are available in Section 4 in the Supporting Information). It is worth mentioning that this value might be at the lower edge of what is required for practical applications since transmission-type plasmonic metasurfaces consisting of metallic structures (e.g., gold or silver) have low efficiency due to the metal loss, especially in the visible range. Although this value can be increased by optimizing design parameters[40] and fabrication process, it has been reported that the maximum experimental value based on single-layer metallic structures is 24.7% in the microwave range.[41] Another solution is to use reflection-type metasurfaces;[37] however, these reflection-type optical devices are generally less popular than transmission-type devices for practical applications. Fortunately, the dielectric metasurfaces have been demonstrated to possess high conversion efficiency since they do not suffer from the Ohmic loss in metal.[19,42] To achieve high conversion efficiency, the dielectric metasurface is an ideal candidate for the proposed device with helicity-dependent functionality.

As mentioned above, half of the nanorods in the merged metasurface contribute to the background noise when the metasurface functions as a hologram or lens. In order to examine to what extent the performance of the merged metasurface is affected by the background noise, a comparison between the separate metasurface before and after merging is shown in **Figure 6** and **Figure 7**. Understandably, the background noise of the reconstructed image of "cat" is higher for the merged metasurface (Figure 6c,d) than that for the separate metasurface hologram (Figure 6a,b). Nevertheless, the intensity of the noise is still much lower than the pattern of "cat" and the outline of the reconstructed image is sharp enough. Figure 7 shows that the focal point of the merged metasurface is nearly unaffected by the background noise. It is interesting to note that the undesired beam (background noise) can be eliminated by utilizing a more sophisticated design approach for the integration of multiple and similar optical functionalities (e.g., two holograms) into one single optical element.[43] However, it is very challenging to completely eliminate the background noise for the multifunction device with totally different functionalities in this project due to the on-axis design.

Another interesting fact is that the virtual image and the real image always coexist in the designed metasurface design. For example, a real focal point on the transmission side and a virtual hologram image ("cat") on the incidence side can be clearly observed when the incident/detected light is RCP/LCP. Similarly, a real hologram image on the transmission side and

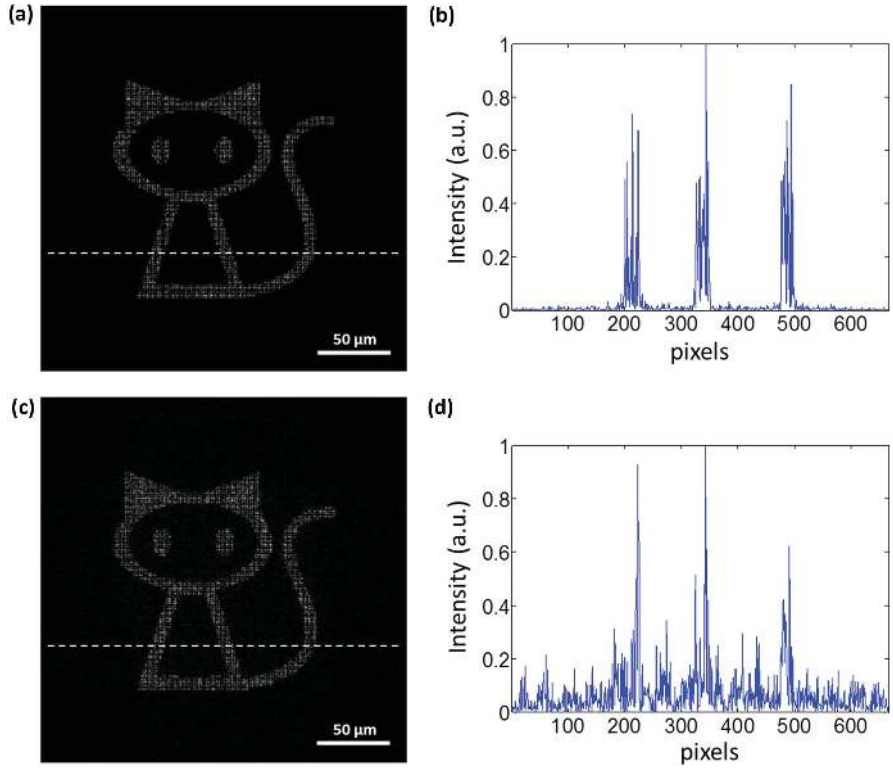

Figure 6. Comparison of simulation images of "cat" for the metasurface hologram before and after merging with the metalens. a) The reconstructed image and b) the corresponding normalized intensity profile along the dashed line shown in (a) before merging. Panels (c) and (d) correspond to the simulation results after merging.

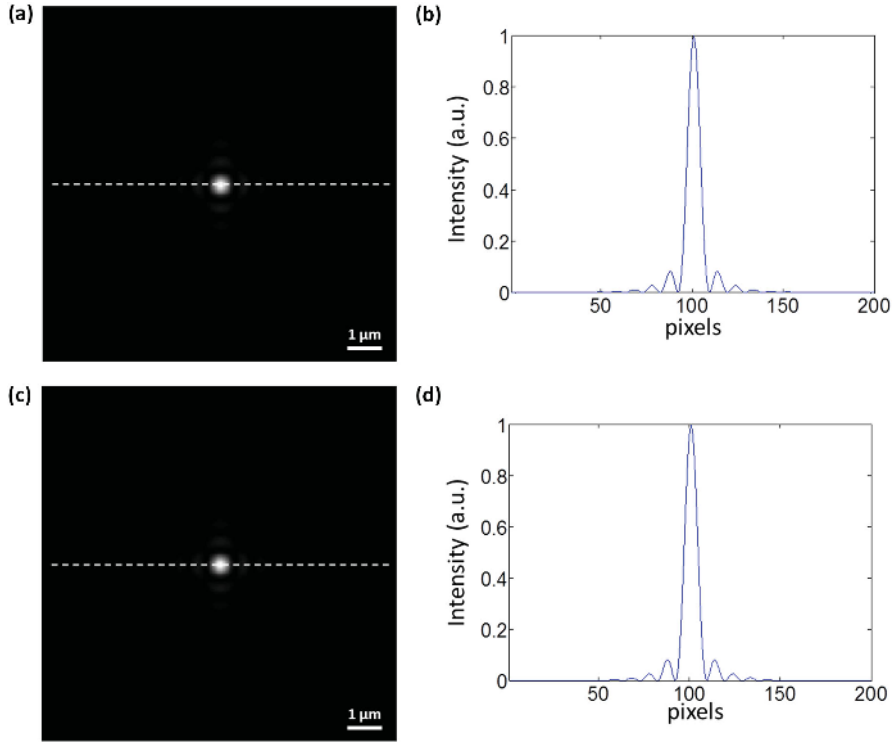

Figure 7. Comparison of simulation results of the light spot in the focal plane for the metalens before and after merging with the metasurface hologram. a) The simulated focal point and b) the corresponding normalized intensity profile along the dashed line shown in (a) before merging. Panels (c) and (d) correspond to the simulation results after merging.

a virtual focal point on the incidence side will appear when the light combination RCP/LCP is changed to LCP/RCP.

5. Conclusion

In conclusion, we have experimentally demonstrated a straightforward approach for designing and integrating multiple optical functions into a single element. The two independent functionalities of a hologram and a lens on the same metasurface device are interchangeable, depending on the helicity of the incident light. Benefiting from arbitrary phase control and uniform scattering amplitude from different nanorods, the metasurface device may pave the way of creating more compact, broadband, and versatile optical components for integrated optics. This type of metasurface device opens a new avenue to achieve a high density of functionality, effectively scaling down the size of photonic systems.

Supporting Information

Supporting Information is available from the Wiley Online Library or from the author.

Acknowledgements

D.W. and S.C. contributed equally to this work. X.C. and S.Z. acknowledge the Engineering and Physical Sciences Research Council of the United Kingdom (Grant Ref: EP/M003175/1 and EP/J018473/1). X.C. also acknowledges the support from Renishaw-Heriot Watt Strategic Alliance. E.Y.B.P. would like to thank the support from Research Grant Council of Hong Kong under CUHK1/CRF/12G. The licence on this manuscript was changed after publication, on February 17, 2016.

Received: September 8, 2015
Revised: October 11, 2015
Published online: November 17, 2015

[1] L. Chen, D. Zhao, *Opt. Express* **2006**, *14*, 8552.
[2] P. J. Winzer, *Nat. Photonics* **2014**, *8*, 345.
[3] Y. Tu, G. Zhang, Z. Zhai, J. Xu, *Phys. Rev. A* **2009**, *80*, 033816–1.
[4] T. Zentgraf, J. Valentine, N. Tapia, J. Li, X. Zhang, *Adv. Mater.* **2010**, *22*, 2561.
[5] N. Zhu, Y. Wang, J. Liu, J. Xie, H. Zhang, *Opt. Express* **2009**, *17*, 13418.
[6] F. Xu, J. E. Ford, Y. Fainman, *Appl. Opt.* **1995**, *34*, 256.
[7] J. E. Ford, F. Xu, K. Urquhart, Y. Fainman, *Opt. Lett.* **1993**, *18*, 456.
[8] N. Nieuborg, A. Kirk, B. Morlion, H. Thienpont, I. Veretennicoff, *Appl. Opt.* **1997**, *36*, 4681.
[9] F. Xu, C.-C. Cheng, A. Scherer, R.-C. Tyan, P.-C. Sun, Y. Fainman, *Opt. Lett.* **1996**, *21*, 1513.
[10] W. Yu, T. Konishi, T. Hamamoto, H. Toyota, T. Yotsuya, Y. Ichioka, *Appl. Opt.* **2002**, *41*, 96.
[11] N. F. Yu, P. Genevet, M. A. Kats, F. Aieta, J. P. Tetienne, F. Capasso, Z. Gaburro, *Science* **2011**, *334*, 333.
[12] X. Z. Chen, L. L. Huang, H. Muhlenbernd, G. X. Li, B. F. Bai, Q. F. Tan, G. F. Jin, C. W. Qiu, S. Zhang, T. Zentgraf, *Nat. Commun.* **2012**, *3*, 1198.
[13] X. J. Ni, N. K. Emani, A. V. Kildishev, A. Boltasseva, V. M. Shalaev, *Science* **2012**, *335*, 427.
[14] X. B. Yin, Z. L. Ye, J. Rho, Y. Wang, X. Zhang, *Science* **2013**, *339*, 1405.
[15] S. L. Sun, Q. He, S. Y. Xiao, Q. Xu, X. Li, L. Zhou, *Nat. Mater.* **2012**, *11*, 426.
[16] S. C. Jiang, X. Xiong, Y. S. Hu, Y. H. Hu, G. B. Ma, R. W. Peng, C. Sun, M. Wang, *Phys. Rev. X* **2014**, *4*, 021026–1.
[17] V. Y. Kildishev, A. Boltasseva, V. M. Shalaev, *Science* **2013**, *339*, 1289.
[18] Y. B. Li, X. Wan, B. G. Cai, Q. Cheng, T. J. Cui, *Sci. Rep.* **2014**, *4*, 6921.
[19] D. Lin, P. Fan, E. Hasman, M. L. Brongersma, *Science* **2014**, *345*, 298.
[20] J. Scheuer, Y. Yifat, *Nat. Nanotechnol.* **2015**, *10*, 296.
[21] Y. Zhao, M. A. Belkin, A. Alu, *Nat. Commun.* **2012**, *3*, 870.
[22] N. K. Grady, J. E. Heyes, D. R. Chowdhury, Y. Zeng, M. T. Reiten, A. K. Azad, A. J. Taylor, D. A. R. Dalvit, H.-T. Chen, *Science* **2013**, *340*, 1304.
[23] S. Larouche, Y.-J. Tsai, T. Tyler, N. M. Jokerst, D. R. Smith, *Nat. Mater.* **2012**, *11*, 450.
[24] Y. Yifat, M. Eitan, Z. Iluz, Y. Hanein, A. Boag, J. Scheuer, *Nano Lett.* **2014**, *14*, 2485.
[25] X. Li, S. Xiao, B. Cai, Q. He, T. J. Cui, L. Zhou, *Opt. Lett.* **2012**, *37*, 4940.
[26] A. Pors, M. G. Nielsen, R. L. Eriksen, S. I. Bozhevolnyi, *Nano Lett.* **2013**, *13*, 829.
[27] W. T. Chen, K. Y. Yang, C. M. Wang, Y. W. Huang, G. Sun, I. D. Chiang, C. Y. Liao, W. L. Hsu, H. T. Lin, S. Sun, L. Zhou, A. Q. Liu, D. P. Tsai, *Nano Lett.* **2014**, *14*, 225.
[28] Y. Montelongo, J. O. Tenorio-Pearl, W. I. Milne, T. D. Wilkinson, *Nano Lett.* **2014**, *14*, 294.
[29] N. Yu, F. Capasso, *Nat. Mater.* **2014**, *13*, 139.
[30] M. V. Berry, *Proc. R. Soc. A* **1984**, *392*, 45.
[31] M. Kang, T. H. Feng, H. T. Wang, J. S. Li, *Opt. Express* **2012**, *20*, 15882.
[32] D. Wen, F. Yue, S. Kumar, Y. Ma, M. Chen, X. Ren, P. E. Kremer, B. D. Gerardot, M. R. Taghizadeh, G. S. Buller, X. Chen, *Opt. Express* **2015**, *23*, 10272.
[33] F. Gori, *Opt. Lett.* **1999**, *24*, 584.
[34] Y. Yirmiyahu, A. Niv, G. Biener, V. Kleiner, E. Hasman, *Opt. Lett.* **2006**, *31*, 3252.
[35] L. L. Huang, X. Z. Chen, H. Muhlenbernd, G. X. Li, B. F. Bai, Q. F. Tan, G. F. Jin, T. Zentgraf, S. Zhang, *Nano Lett.* **2012**, *12*, 5750.
[36] F. Aieta, P. Genevet, M. A. Kats, N. F. Yu, R. Blanchard, Z. Gahurro, F. Capasso, *Nano Lett.* **2012**, *12*, 4932.
[37] G. Zheng, H. Mühlenbernd, M. Kenney, G. Li, T. Zentgraf, S. Zhang, *Nat. Nano* **2015**, *10*, 308.
[38] P. Hariharan, *Optical Holography Principles, Techniques, and Applications*, 2nd ed., Cambridge University Press, New York **1996**.
[39] F. F. Wei, Z. W. Liu, *Nano Lett.* **2010**, *10*, 2531.
[40] W. J. Luo, S. Y. Xiao, Q. He, S. L. Sun, L. Zhou, *Adv. Opt. Mater.* **2015**, *3*, 1102.
[41] X. M. Ding, F. Monticone, K. Zhang, L. Zhang, D. L. Gao, S. N. Burokur, A. de Lustrac, Q. Wu, C. W. Qiu, A. Alu, *Adv. Mater.* **2015**, *27*, 1195.
[42] E. Hasman, V. Kleiner, G. Biener, A. Niv, *Appl. Phys. Lett.* **2003**, *82*, 328.
[43] D. Wen, F. Yue, G. Li, G. Zheng, K. Chan, S. Chen, M. Chen, K. F. Li, P. W. H. Wong, K. W. Cheah, E. Yue Bun Pun, S. Zhang, X. Chen, *Nat. Commun.* **2015**, *6*, 8241.